RESEARCH ARTICLE
SPACE PHYSICS

Earth and Planetary Physics
9: 1163–1170, 2025
doi: 10.26464/epp2025075

Statistical study of auroral variability under different solar wind conditions based on classification using deep learning techniques

ZhiYuan Shang[1,2], ZhongHua Yao[1,2*], Jian Liu[3,4,5*], LinLi Xu[6,7], Yan Xu[1,2], BinZheng Zhang[8], RuiLong Guo[9], Yuan Yu[8], and Yong Wei[1,2]

[1]Key Laboratory of Earth and Planetary Physics, Institute of Geology and Geophysics, Chinese Academy of Sciences, Beijing 100029, China;

[2]College of Earth and Planetary Sciences, University of Chinese Academy of Sciences, Beijing 100029, China;

[3]Weihai Institute for Interdisciplinary Research, Shandong University, Weihai Shandong 264200, China;

[4]SDU-ANU Joint Science College, Shandong University, Weihai Shandong 264200, China;

[5]School of Nuclear Science and Technology, University of Science and Technology of China, Hefei 230000, China;

[6]Anhui Province Key Laboratory of Big Data Analysis and Application, School of Computer Science and Technology, University of Science and Technology of China, Hefei 230000, China;

[7]Anhui Province Key Laboratory of Big Data Analysis and Application, School of Computer Science and Technology, State Key Laboratory of Cognitive Intelligence, Hefei 230000, China;

[8]Department of Earth Sciences, The University of Hong Kong, Hong Kong SAR 999077, China;

[9]Laboratory of Optical Astronomy and Solar-Terrestrial Environment, Institute of Space Sciences, School of Space Science and Physics, Shandong University, Weihai Shandong 264200, China

Key Points:

- ConvNeXt deep learning model achieves 99.4% accuracy in automated auroral image classification.
- Auroral occurrence rates decrease with latitude and vary systematically with solar wind activity phases.
- Statistical analysis reveals strong correlation between K-index geomagnetic activity and auroral occurrence patterns.

Citation: Shang, Z. Y., Yao, Z. H., Liu, J., Xu, L. L., Xu, Y., Zhang, B. Z., Guo, R. L., Yu, Y., and Wei, Y. (2025). Statistical study of auroral variability under different solar wind conditions based on classification using deep learning techniques. *Earth Planet. Phys.*, *9*(6), 1163–1170. http://doi.org/10.26464/epp2025075

Abstract: In this investigation, we meticulously annotated a corpus of 21,174 auroral images captured by the THEMIS All-Sky Imager across diverse temporal instances. These images were categorized using an array of descriptors such as 'arc', 'ab' (aurora but bright), 'cloudy', 'diffuse', 'discrete', and 'clear'. Subsequently, we utilized a state-of-the-art convolutional neural network, ConvNeXt (Convolutional Neural Network Next), deploying deep learning techniques to train the model on a dataset classified into six distinct categories. Remarkably, on the test set our methodology attained an accuracy of 99.4%, a performance metric closely mirroring human visual observation, thereby underscoring the classifier's competence in paralleling human perceptual accuracy. Building upon this foundation, we embarked on the identification of large-scale auroral optical data, meticulously quantifying the monthly occurrence and Magnetic Local Time (MLT) variations of auroras from stations at different latitudes: RANK (high-latitude), FSMI (mid-latitude), and ATHA (low-latitude), under different solar wind conditions. This study paves the way for future explorations into the temporal variations of auroral phenomena in diverse geomagnetic contexts.

Keywords: aurora classification; deep learning; user graphical interface

1. Introduction

Auroras, often described as natural luminous displays, manifest when solar wind—streams of charged particles emanating from the Sun—interacts intricately with Earth's magnetosphere and atmospheric layers. Periodically, the Sun discharges copious amounts of charged particles and magnetic flux, disrupting the Earth's magnetic field and atmospheric equilibrium. Such solar disturbances, upon reaching Earth, can induce pronounced alterations in both the planet's magnetic field and its atmospheric conditions, with these effects being particularly pronounced in polar regions. Auroras serve as a visual indicator of these geomagnetic variations at high latitudes, a phenomenon well-documented in the literature (Akasofu, 1981; Baker et al., 1996). Hence, accurate identification and classification of various auroral forms is crucial for enhancing our understanding of the dynamics within the

First author: Z. Y. Shang, shangzhiyuan21@mails.ucas.ac.cn
Correspondence to: Z. H. Yao, z.yao@mail.iggcas.ac.cn
J. Liu, liu_jian@sdu.edu.cn
Received 26 SEP 2024; Accepted 28 MAY 2025.
First Published online 14 JUL 2025.

Earth's magnetosphere.

In addition to contributions from specialized scientific entities engaged in auroral photography, a burgeoning corpus of auroral imagery is amassed annually by citizen scientists. Collectively, these enthusiasts, equipped with advanced photographic tools, generate millions of auroral images each year. Given this voluminous database, manual identification through unaided visual analysis is not only impractical but would also be inefficient. The inherently variable and complex nature of auroral structures further exacerbates this challenge, underscoring the necessity for automated identification systems. Such tools are indispensable for enabling researchers to methodically, objectively, and consistently analyze pertinent images.

The integration of these automated systems paves the way for more sophisticated statistical analyses. For instance, discerning probabilistic distributions across various auroral classifications is instrumental in investigating the temporal dynamics of auroras under distinct geomagnetic scenarios. Moreover, automated classifications enable in-depth statistical examinations of the ionosphere–magnetosphere environment. By analyzing the frequency and development of specific auroral types, such as patchy auroras, alongside the statistical investigation of phenomena like pitch angle scattering resulting from wave–particle interactions within the ionosphere–magnetosphere system, a more comprehensive understanding of these complex geophysical processes can be achieved.

To date, scientists have leveraged statistical machine learning and deep learning techniques to automate the classification of auroral phenomena. Early endeavors in this field utilized methods such as the K-NN (K-Nearest Neighbour) algorithm (Syrjäsuo and Donovan, 2002, 2004), the Hidden Markov Model (Yang QJ et al., 2012), and the Support Vector Machine (SVM) (Rao J et al., 2014). Initially, these methods faced major limitations—a restricted range of identifiable auroral categories, and suboptimal accuracy rates. To enhance precision, subsequent studies employed a combination of multiple algorithms, particularly for classifying daytime auroras (Fu R et al., 2009; Wang Q et al., 2010; Zhong YF et al., 2018).

As the field evolved, deep learning methods increasingly came to the forefront in auroral classification. Clausen and Nickisch (2018) utilized the Ridge classifier to categorize auroras into six distinct types: arc, clear/no aurora, diffuse, discrete, moon, and cloudy, achieving an accuracy of 81.7 ± 0.1%. Notably, the model's performance in distinguishing aurora from non-aurora images reached an impressive 95.6 ± 0.03% accuracy. Kvammen (2020) expanded the auroral taxonomy to seven labels, including broken, colored, arc, discrete, patchy, rimmed, and faint, and demonstrated that the ResNet-50 algorithm outperformed traditional machine learning methods with a 92% accuracy rate. In a more recent study, Guo ZX et al. (2022) introduced eight auroral labels and compared the performance of the DenseNet and EfficientNet algorithms. Shang ZY et al. (2023) further advanced the field by implementing the ConvNeXt and Transformer algorithms in auroral classification, achieving a remarkable 98% accuracy. Thus, it is evident that the current tools and methodologies for auroral recognition are highly sophisticated and effective.

Despite significant progress with deep learning methods in auroral image classification, several limitations remain. First, traditional machine learning methods, such as K-NN and SVM, suffer from high computational complexity and suboptimal generalization when applied to large-scale, high-dimensional auroral image datasets. Specifically, in auroral image classification tasks, class imbalance often reduces classification accuracy, and traditional methods often lack the flexibility of modern deep learning approaches to handle severe class imbalance adaptively. Furthermore, although deep learning models like ResNet-50 are effective for image data, their deep architectures, designed primarily for static image classification, may struggle to capture temporal correlations in dynamically changing auroral sequences, potentially overlooking subtle morphological variations over time.

To address these limitations, this study employs the ConvNeXt algorithm (Liu Z et al., 2022), a modernized convolutional network optimized for enhanced hierarchical feature extraction. Compared to traditional convolutional models, ConvNeXt benefits from larger kernel sizes and adaptive feature fusion mechanisms, enabling superior representation of multi-scale auroral structures. The larger kernels help capture broader spatial features, while adaptive fusion mechanisms combine information from different scales effectively. Combined with advanced data augmentation strategies, ConvNeXt's enhanced feature representation capability enables it to better generalize on imbalanced auroral datasets. Furthermore, ConvNeXt's robustness in processing high-resolution All-Sky Imager (ASI) images is enhanced by its hierarchical design, which progressively reduces spatial resolution at certain layers while expanding feature dimensions at others, enabling efficient processing without losing critical image details.

By adopting ConvNeXt, this study builds on previous research while introducing innovations in classification accuracy, computational efficiency, and data handling. These advancements provide a more reliable and efficient approach to automated auroral classification, thereby contributing to a deeper understanding of the dynamic nature of auroras and of magnetosphere–ionosphere interactions.

2. Methodology

Utilizing auroral imagery from THEMIS All Sky Imagers, this study meticulously selected auroral images from three stations: RANK, FSMI, and ATHA, representing datasets from different latitudes. The images encompass the Februarys of the years 2011, 2014, 2016, and 2019. Auroral data from February were chosen for two main reasons. First, winter is the season with the most abundant observations of auroras of even the rarest sorts; second, selecting February helps to make the study more quantitative, as it avoids excessive fluctuations in auroral occurrence frequencies due to monthly variations, which could affect our analysis of auroral variations under different solar wind conditions. All ground stations in the THEMIS network are equipped to capture auroral phenomena within the wavelength range of 400–700 nm, with the remarkable capability of recording auroral characteristics at intervals of about 3 seconds. Consequently, these four years of February data allowed us to choose a total of 4,669,163 auroral images for analysis at this maximum resolution. From this extensive dataset, 21,174 images were manually labeled and randomly divided into training and test sets in an 8:2 ratio.

The labeling criteria, as delineated in Clausen and Nickisch (2018) and Nanjo et al. (2022), encompassed categories such as ab (aurora but bright), arc, clear, cloudy, diffuse, and discrete. Figure 1 illustrates these categories. The 'arc' category is characterized by stripes extending east–west, typically observed before the aurora assumes a more arc-like appearance (Karlsson et al., 2020). 'Discrete' auroras are relatively brighter, attributed to their higher energy emission. 'Diffuse' auroras, in contrast, are fainter and challenging to discern with the naked eye during daylight, predominantly observed post-midnight. The categories of arc, diffuse, and discrete are classified as high-quality clear auroras, unaffected by solar or cloud interference. 'Clear' is defined as the absence of observable auroras. These four categories are collectively considered observable auroras for subsequent calculations of auroral occurrence rates.

'Ab' is designated for auroras that are partially visible or partially obscured by solar or lunar interference. 'Cloudy' pertains to auroras hindered by cloud cover. These two classifications are categorized as noisy auroras. The methodology for calculating the auroral occurrence rate is delineated as follows:

$$\left(w_{(\mathrm{arc})}+w_{(\mathrm{diffuse})}+w_{(\mathrm{discrete})}\right)/w_{(\mathrm{Observableclasses})}.$$

Humans naturally improve our ability to recognize phenomena by constantly noting, at each new instance, more and more characteristics of a particular phenomenon. Deep learning proposes to simulate this feature of the human nervous system's ability to perceive, categorize, and recall phenomena. Similarly, machine learning recognizes objects through pre-determined features extracted from raw data (Guyon and Elisseeff, 2003). In contrast, deep learning trains on large datasets and automatically extracts key features without defining those features in advance (Lecun et al., 2015).

To classify auroral images, we use a Deep Neural Network (DNN) with a convolutional layer. This layer has many filters that apply convolutions to the input layer and extract image features. The deeper the network goes, the larger the receptive field on the output feature map becomes. This means the features go from specific to general. In the end, a fully connected layer gives us the probabilities for each category.

Based on this, we have chosen the newly developed ConvNeXt algorithm and applied it to our work on Aurora classification. ConvNeXt is a family of Convolutional Neural Networks (ConvNets) designed for image classification and other visual recognition tasks. The ConvNeXt model achieves high efficiency and scalability because it was designed to accommodate hardware and software limitations; it uses techniques such as grouped convolution, deep separable convolution, attention mechanisms, and multi-scale feature fusion to reduce computational and memory costs while maintaining or improving accuracy. The detailed structure of the model can be found in Supplementary Material. The model can be scaled up or down by adjusting the number and size of grouped convolutional layers, depending on the dataset and the task. It is also capable of scaling hardware platforms such as CPUs, GPUs, TPUs, and mobile devices using different implementation strategies and optimization techniques.

3. Results

In this study, a staggering total of 4,669,163 images were captured from three distinct stations—RANK (lat: 62.82, lon: 267.89; maglat: 72.20, maglon: 336.19), FSMI (lat: 60.03, lon: 248.07; maglat: 67.29, maglon: 307.05), and ATHA (lat: 54.71, lon: 246.69; maglat: 61.88, maglon: 307.21)—during February of the years 2011, 2014, 2016, and 2019. From this extensive collection, a subset of 21,174 images was meticulously selected and labeled, manually, to facilitate the training and evaluation of the ConvNeXt model. The allocation of images into training and test sets adhered to an 8:2 ratio, with the distribution of random seeds detailed in Table 1. To enhance the model's generalization capabilities, the selection process deliberately included a requirement

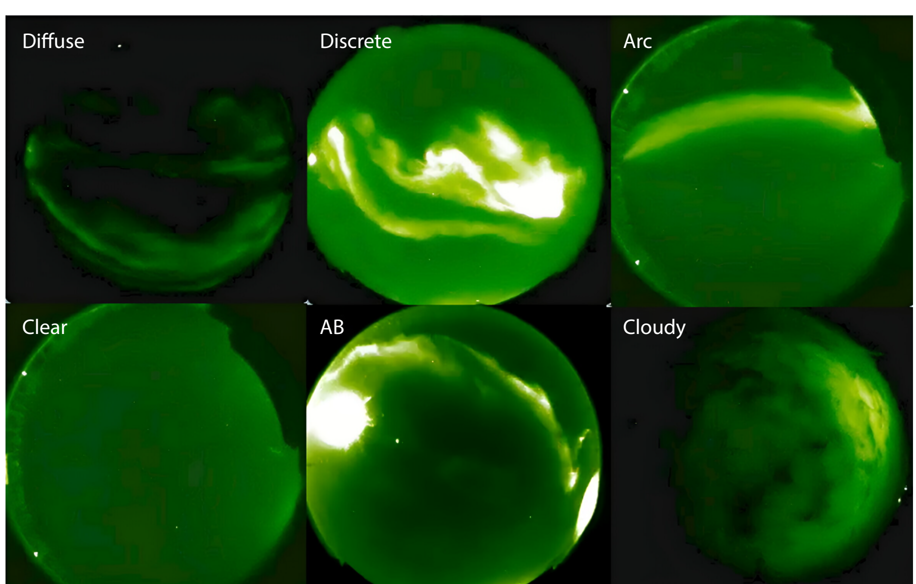

Figure 1. Example images of 6 classes of aurora from an all-sky camera.

Table 1. Several images per class were used for training and testing the model.

Label	AB	Arc	Clear	Cloudy	Diffuse	Discrete
Training	2107	1357	1454	2246	5795	3981
Test	527	339	363	561	1449	995

that the time intervals between chosen images would be diverse.

The efficacy of the trained ConvNeXt model was visually represented through a confusion matrix, as depicted in Figure 2. This matrix illustrates the classification accuracy, for each identified category, against the test data. Notably, the model achieved a remarkable 100% accuracy in identifying the 'ab' category from the total of 527 'ab' images within the test dataset. The matrix's panels, where the true and predicted labels coincide (indicating correct classifications), are predominantly red, signifying a high level of classification accuracy. Overall, the model attained an impressive average accuracy rate of 99.4%.

Figure 3 showcases a pre-softmax two-dimensional visualization of the aurora dataset's test data as processed by the ConvNeXt model. This visualization was achieved by employing the t-distributed stochastic neighbor embedding (T-SNE) technique for dimensionality reduction, a method originally proposed by van der Maaten and Hinton (van der Maaten and Hinton, 2008). Within this figure, various actual images corresponding to the two-dimensional points are also included for reference. This two-dimensional mapping plays a pivotal role in the network's decision-making process as it classifies each image. Observations from this figure reveal a notable distinction in the spatial separation among certain classes. On the other hand, a few classes exhibit a degree of overlap, aligning with the observations made in Figure 2.

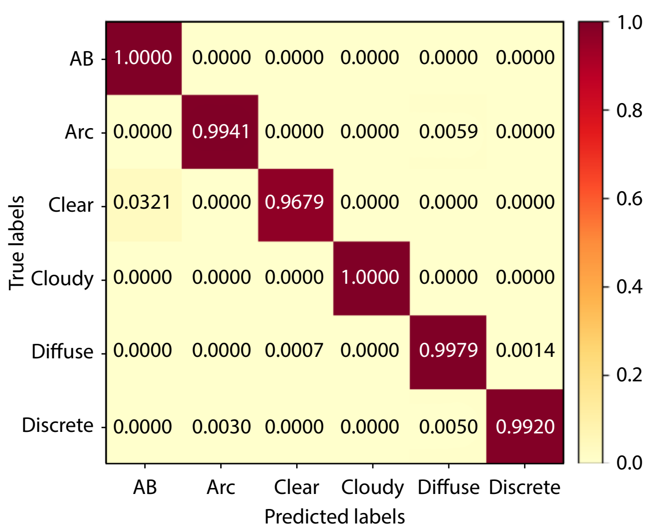

Figure 2. Classification results of the test dataset by the trained ConvNeXt model. The diagonal elements represent the percentage of correctly classified images for each class, while the off-diagonal elements indicate the percentage of images from a given class that were misclassified as other classes.

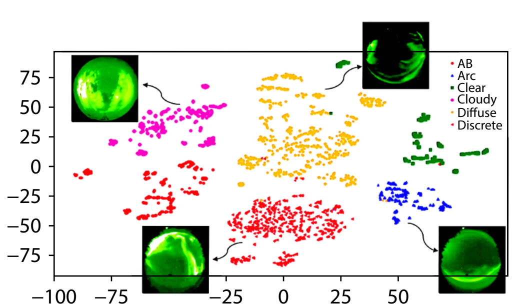

Figure 3. This figure shows the presoftmax representation of the auroral test data generated by the ConvNeXt network, projected to two dimensions using T-SNE. Images of some of the categories are also shown in the figure.

Meanwhile, Figure 4 presents the two-dimensional visualization of the aurora dataset test data after dimensionality reduction using UMAP (Uniform Manifold Approximation and Projection). UMAP is a non-linear dimensionality reduction technique designed to preserve the local neighborhood structure of the data. Compared to T-SNE, UMAP offers higher computational efficiency and better preservation of global structures. We can observe that most classes exhibit clear spatial separation, particularly the "Diffuse", "Discrete", and "Cloudy" classes, where data points are more concentrated in specific regions, suggesting a higher discriminative power in the feature space.

To thoroughly investigate the variability and evolutionary patterns of auroras under diverse solar wind conditions, our study focused strategically on data gathered from three distinct stations, RANK, FSMI, and ATHA, which are representative of high, mid, and low-latitude regions, respectively. The data selected for analysis encompassed four specific periods: February 2011, 2014, 2016, and 2019. These periods were chosen deliberately as they align with the rising, peak, declining, and minimum phases of solar wind activity. The categorization of these four distinct phases was based on sunspot numbers. For an in-depth understanding of the fluctuation in sunspot numbers and the geographical distribution of the auroral stations, readers are referred to Supplementary Material, particularly Figures S1 and S2.

Figure 5 summarizes results of using the ConvNeXt model to classify and analyze auroral occurrences. Our analysis reveals distinct temporal and latitudinal variations in auroral occurrences:

(1) **February 2011 (Rising Solar Wind Activity):** High-latitude regions exhibited the highest auroral occurrence at 05 UT, which roughly corresponds to 22 MLT. while mid-latitudes peaked at 09

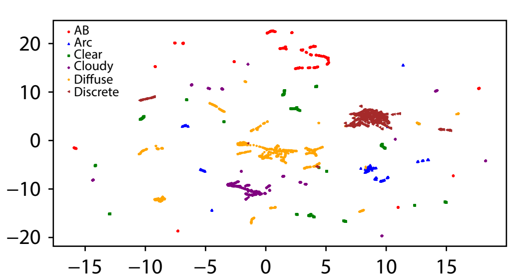

Figure 4. Two-dimensional visualization of the aurora dataset test data using UMAP dimensionality reduction.

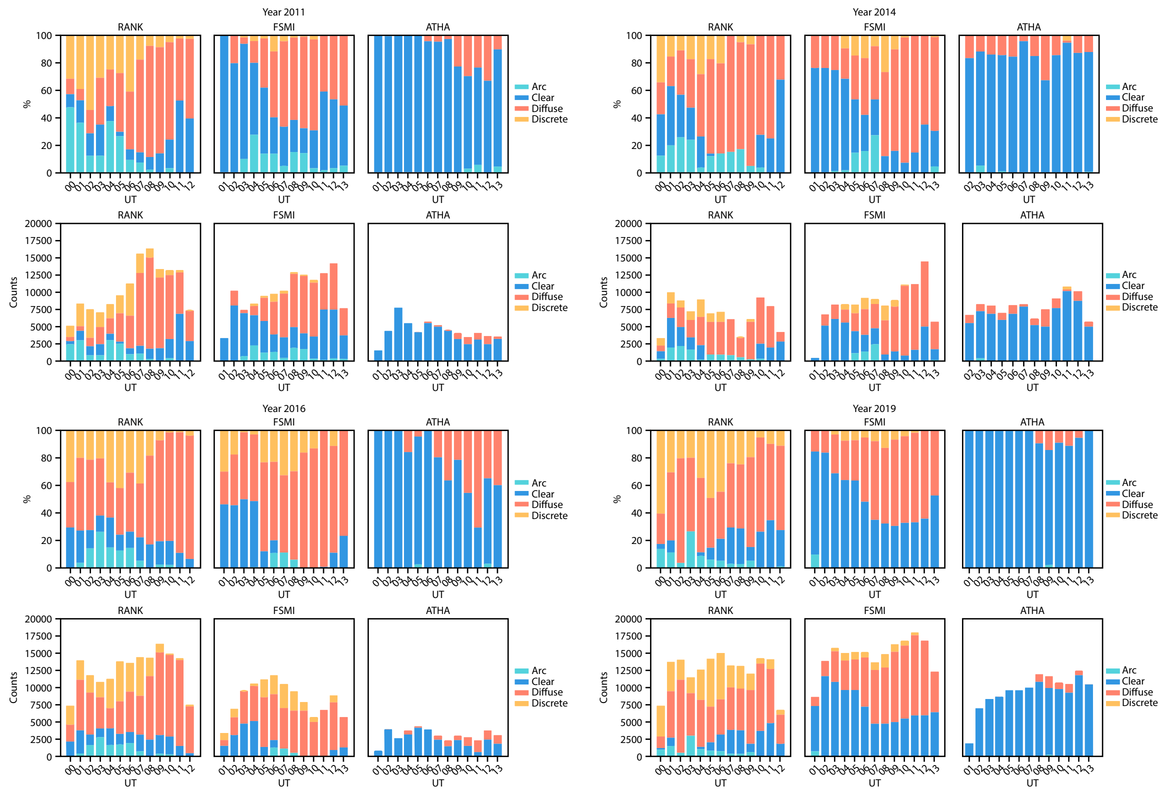

Figure 5. These histograms illustrate the distribution of observable aurora categories across four different time periods. The data are organized chronologically, representing the months of February in 2011, 2014, 2016, and 2019. Along the horizontal axis, from left to right, the histograms present data from stations located at different latitudes: the high-latitude RANK station, the mid-latitude FSMI station, and the low-latitude ATHA station.

UT (~00 MLT). Low-latitudes experienced minimal auroral activity. The frequency of discrete auroras (including arcs and discrete types) reached a zenith at 04 UT (~21 MLT) and gradually tapered off thereafter. Diffuse auroras showed a broad distribution across multiple MLTs, peaking at 08 UT (~01 MLT).

(2) **February 2014 (Maximum Solar Wind Activity):** This period marked a heightened observation of discrete auroras around 04–06 UT (~21–23 MLT) in high-latitudes and mid-latitudes; auroras continued to appear until 10 UT in mid-latitudes. Diffuse auroras were greatest after 21 UT, especially at 09–10 UT (~00–01 MLT), reaching a maximum at high and mid-latitudes. These observations align with prior studies (Syrjäsuo and Donovan, 2004; Jones et al., 2011; Partamies et al., 2017; Bland et al., 2019; Nishimura et al., 2020). The diffuse auroras, thought to originate from magnetospheric waves, showed a temporal correlation with their theoretical source (Li W et al., 2009; Nishimura et al., 2010; Jaynes et al., 2013; Kasahara et al., 2018; Fukizawa et al., 2018, 2020; Hosokawa et al., 2020). As can be seen from the results above, there is good agreement between observations at high and mid-latitudes.

(3) **February 2016 (Early Declining Phase of Solar Cycle):** We observed an increased auroral occurrence, especially at mid-latitudes. High and mid-latitude stations recorded predominantly arc and discrete auroras, indicating active geomagnetic conditions, confirmed by the K-index in Figure 6b.

(4) **February 2019 (Minimum Solar Wind Activity):** The auroral occurrence at all stations, except high-latitudes, was notably lower compared to other periods, underscoring the influence of latitude on auroral activity. Trends in auroral subclasses over time reflect the stability and consistency of the statistical results.

Utilizing the classifications determined by the ConvNeXt model, we computed the aurora occurrence rates at different latitudes, as depicted in Figure 6a. This analysis reveals a consistent pattern: high-latitude stations exhibited higher aurora occurrence rates compared to mid-latitude stations, which in turn displayed higher rates than low-latitude stations. The geographic constraints of low-latitude regions result in less pronounced fluctuations in aurora occurrence, even during periods of heightened solar wind activity and during the early declining phase of solar cycles.

In Figure 6b, we present the temporal variation of the mean K-index, a measure of geomagnetic activity. This graph demonstrates a notable correlation between the fluctuations in aurora occurrence rates and the K-index, suggesting a strong link between geomagnetic disturbances and auroral activities across different latitudes.

In this research, we have successfully quantified the monthly and Universal Time (UT) variations in auroral occurrence rates at the RANK, FSMI, and ATHA stations. While this statistical analysis provides a broad overview, it does not enable precise identification of auroral types at specific times. To address this limitation, we have developed an innovative user graphical interface. This interface facilitates real-time identification of auroral activities, allowing users to pinpoint the type of aurora present at any given moment.

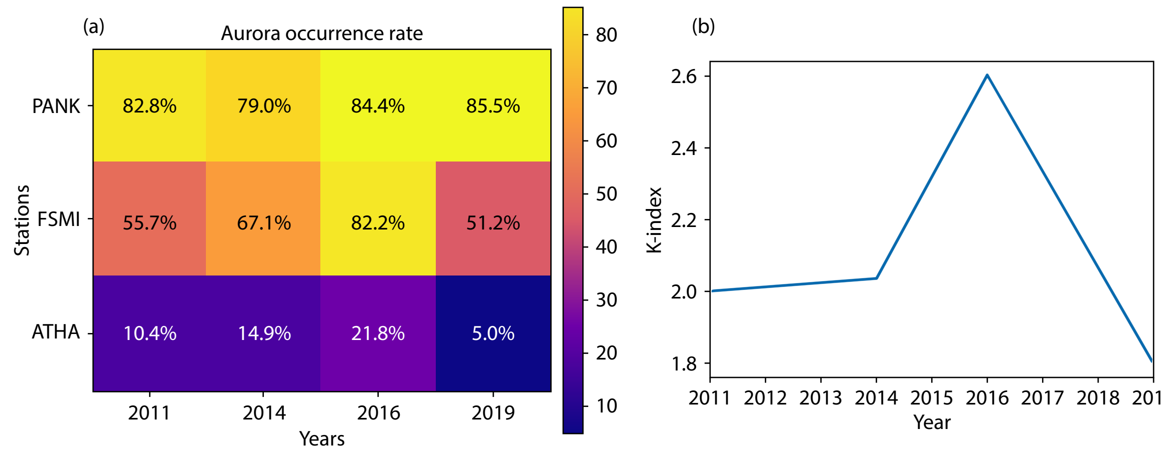

Figure 6. (a) Monthly auroral occurrence rate for the three stations over four periods, with auroral incidence defined as the number of auroral images divided by the total number of images in the dataset. Yellow panels indicate high auroral occurrence rates; blue panels indicate low auroral occurrence rates. (b) Mean K-index versus time.

Figure 7 showcases this interface, and for those interested in exploring or utilizing this tool, the relevant source code is available at GitHub-auroragui.py.

4. Discussion

In our investigation, we employed the ConvNeXt algorithm, a cutting-edge deep-learning technique available in various versions. Due to computational constraints, we opted for the ConvNeXt-tiny variant, which has fewer parameters. Despite this, we achieved a high accuracy of 99.4%, underscoring the suitability of Deep Neural Networks (DNNs) for aurora classification. It is plausible that selecting a more extensive version of ConvNeXt with more parameters might have further enhanced our results. Additionally, we implemented transfer learning, which offered the dual benefits of reducing model training time and obviating the need for a larger dataset.

Our analysis was confined to temporal data from just three stations; performance evaluations on data from additional stations remain incomplete. A limitation of the THEMIS instrument is its focus on capturing auroral images in the visible range of 400–700 nm, excluding other spectral ranges and colors of auroral images. Moreover, to minimize the impact of blurred images on model performance, our training and testing datasets consisted of unequivocal auroral images. As McKay and Kvammen (2020) have noted, human categorization of ambiguous images can be biased and subjective. Thus, expecting DNNs to accurately classify such images when even experts might disagree on their categorization, is unrealistic.

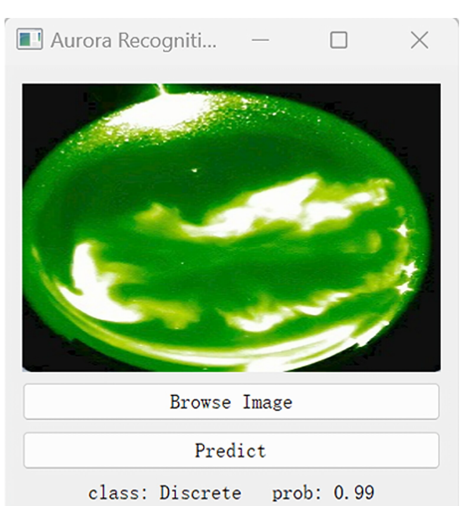

Figure 7. Aurora recognition user graphical interface. After importing an aurora image, click on the prediction to obtain the class of the aurora and the corresponding probability value.

In our auroral occurrence statistics, we considered only data from February of each chosen year. Future work will expand the scope to include more stations and additional auroral categories such as colored auroras (Størmer, 1929; Shiokawa et al., 2019) and stable auroral red (SAR) arcs (Rees and Roble, 1975; Mendillo et al., 2016). This broader approach will enable us to analyze annual, monthly, and UT variability in auroral occurrences across different latitudes. We aim to align the electromagnetic and plasma environments in our simulations more closely with real-time values, enhancing our understanding of the interplay between auroral pattern production mechanisms and magnetotail processes. This effort will also help refine our user graphical interface.

5. Conclusion

This paper elucidates a successful classification of auroras using the ConvNeXt algorithm across six categories: ab, arc, clear, cloudy, diffuse, and discrete. Achieving an impressive accuracy rate of 99.4%, the study further delves into statistical analysis of auroral variability with about Universal Time (UT) at high, mid, and low-latitude stations, as well as monthly auroral occurrences. The key findings of our research are summarized as follows:

(1) **Latitudinal Variation:** Independently of the solar wind activity state, auroral occurrences consistently display a higher frequency at high latitudes compared to mid-latitudes, and at mid-latitudes compared to low latitudes, with a notably low overall rate at low latitudes. High-latitude regions are directly connected to the polar

cap and auroral oval, where field-aligned currents (FACs) are most intense. These currents, known as Region 1 (R1) and Region 2 (R2) currents, are driven by the interaction between the solar wind and the magnetosphere. During periods of enhanced solar wind activity, the R1 and R2 currents intensify, leading to increased particle precipitation and auroral emissions in high-latitude regions. In contrast, mid- and low-latitude regions are less directly influenced by these currents, resulting in lower auroral occurrence rates.

(2) **Solar Wind Activity Impact:** The enhanced auroral activity observed at mid-latitudes during the declining phase of the solar cycle, such as in February 2016, can be attributed to alterations in global magnetospheric convection patterns. During this phase, solar wind dynamic pressure and interplanetary magnetic field (IMF) conditions often induce a more stretched and unstable magnetotail configuration. These changes contribute to the occurrence of magnetospheric substorms, which in turn lead to increased particle precipitation at lower latitudes. Furthermore, the expansion of the auroral oval during substorm events facilitates extension of auroral emissions into mid-latitudes. The observed correlation between the K-index and auroral occurrence rates provides additional support for this interpretation.

(3) **Diffuse Aurora Origin:** The occurrence of diffuse auroras, potentially arising from magnetospheric electrons being pitch-angle scattered by whistler mode chorus waves, aligns with the presence of these magnetospheric activities, peaking around 09 UT (~00 MLT) and continuing thereafter.

(4) **Arc and Discrete Aurora Observation:** The predominance of arc and discrete auroras during active geomagnetic storm periods (e.g., 04–06 UT, ~21–23 MLT) is consistent with the enhanced particle precipitation associated with substorms. During substorms, the magnetotail reconnection process accelerates electrons, which then precipitate along magnetic field lines, producing bright, discrete auroral arcs. The observed temporal and spatial distribution of these auroras aligns with the expected behavior of substorm-related particle precipitation.

(5) **Temporal Variation:** A lower occurrence rate of auroras is noted during the early and late parts of the observational day.

These conclusions provide valuable insights into the spatial and temporal variations of auroral events and their correlations with geomagnetic and solar wind variations.

Acknowledgments

This study was supported by the General Program of the National Natural Science Foundation of China (Grant No. 42374212) and the National Magnetic Confinement Fusion Energy Research and Development Program of China (Grant No. 2024YFE03020004). We thank Zhuang Liu for developing the ConvNeXt model, the code for which can be found at https://github.com/facebookresearch/ConvNeXt. Our user GUI code can be found at https://github.com/Ryannok/auroragui/blob/main/auroragui.py. The THEMIS all-sky data are available through the THEMIS website at http://themis.ssl.berkeley.edu.

References

Akasofu, S. I. (1981). Energy coupling between the solar wind and the magnetosphere. *Space Sci. Rev.*, *28*(2), 121–190. https://doi.org/10.1007/BF00218810

Baker, D. N., Pulkkinen, T. I., Angelopoulos, V., Baumjohann, W., and McPherron, R. L. (1996). Neutral line model of substorms: Past results and present view. *J. Geophys. Res.: Space Phys.*, *101*(A6), 12975–13010. https://doi.org/10.1029/95JA03753

Bland, E. C., Partamies, N., Heino, E., Yukimatu, A. S., and Miyaoka, H. (2019). Energetic electron precipitation occurrence rates determined using the Syowa East SuperDARN radar. *J. Geophys. Res.: Space Phys.*, *124*(7), 6253–6265. https://doi.org/10.1029/2018JA026437

Clausen, L. B. N., and Nickisch, H. (2018). Automatic classification of auroral images from the oslo auroral THEMIS (OATH) data set using machine learning. *J. Geophys. Res.: Space Phys.*, *123*(7), 5640–5647. https://doi.org/10.1029/2018JA025274

Fu, R., Li, J., Gao, X. B., and Jian, Y. J. (2009). Automatic aurora images classification algorithm based on separated texture. In *Proceedings of 2009 IEEE International Conference on Robotics and Biomimetics* (pp. 1331–1335). Guilin, China: IEEE. https://doi.org/10.1109/ROBIO.2009.5420722

Fukizawa, M., Sakanoi, T., Miyoshi, Y., Hosokawa, K., Shiokawa, K., Katoh, Y., Kazama, Y., Kumamoto, A., Tsuchiya, F., … Fujii, R. (2018). Electrostatic electron cyclotron harmonic waves as a candidate to cause pulsating auroras. *Geophys. Res. Lett.*, *45*(23), 12661–12668. https://doi.org/10.1029/2018GL080145

Fukizawa, M., Sakanoi, T., Miyoshi, Y., Kazama, Y., Katoh, Y., Kasahara, Y., Matsuda, S., Matsuoka, A., Kurita, S., … Jun, C. W. (2020). Pitch-angle scattering of inner magnetospheric electrons caused by ECH waves obtained with the Arase satellite. *Geophys. Res. Lett.*, *47*(23), e2020GL089926. https://doi.org/10.1029/2020GL089926

Guo, Z. X., Yang, J. Y., Dunlop, M. W., Cao, J. B., Li, L. Y., Ma, Y. D., Ji, K. F., Xiong, C., Li, J., and Ding, W. T. (2022). Automatic classification of mesoscale auroral forms using convolutional neural networks. *J. Atmos. Sol. Terr. Phys.*, *235*, 105906. https://doi.org/10.1016/j.jastp.2022.105906

Guyon, I., and Elisseeff, A. (2003). An introduction to variable and feature selection. *J. Mach. Learn. Res.*, *3*, 1157–1182.

Hosokawa, K., Miyoshi, Y., Ozaki, M., Oyama, S. I., Ogawa, Y., Kurita, S., Kasahara, Y., Kasaba, Y., Yagitani, S., … Fujii, R. (2020). Multiple time-scale beats in aurora: precise orchestration via magnetospheric chorus waves. *Sci. Rep.*, *10*(1), 3380. https://doi.org/10.1038/s41598-020-59642-8

Jaynes, A. N., Lessard, M. R., Rodriguez, J. V., Donovan, E., Loto'Aniu, T. M., and Rychert, K. (2013). Pulsating auroral electron flux modulations in the equatorial magnetosphere. *J. Geophys. Res.: Space Phys.*, *118*(8), 4884–4894. https://doi.org/10.1002/jgra.50434

Jones, S. L., Lessard, M. R., Rychert, K., Spanswick, E., and Donovan, E. (2011). Large-scale aspects and temporal evolution of pulsating aurora. *J. Geophys. Res.: Space Phys.*, *116*(A3), A03214. https://doi.org/10.1029/2010JA015840

Karlsson, T., Andersson, L., Gillies, D. M., Lynch, K., Marghitu, O., Partamies, N., Sivadas, N., and Wu, J. (2020). Quiet, discrete auroral arcs—observations. *Space Sci. Rev.*, *216*(1), 16. https://doi.org/10.1007/s11214-020-0641-7

Kasahara, S., Miyoshi, Y., Yokota, S., Mitani, T., Kasahara, Y., Matsuda, S., Kumamoto, A., Matsuoka, A., Kazama, Y., … Shinohara, I. (2018). Pulsating aurora from electron scattering by chorus waves. *Nature*, *554*(7692), 337–340. https://doi.org/10.1038/nature25505

Kvammen, A., Wickstrøm, K., McKay, D., and Partamies, N. (2020). Auroral image classification with deep neural networks. *J. Geophys. Res.: Space Phys.*, *125*(10), e2020JA027808. https://doi.org/10.1029/2020JA027808

LeCun, Y., Bengio, Y., and Hinton, G. (2015). Deep learning. *Nature*, *521*(7553), 436–444. https://doi.org/10.1038/nature14539

Li, W., Thorne, R. M., Angelopoulos, V., Bortnik, J., Cully, C. M., Ni, B., LeContel, O., Roux, A., Auster, U., and Magnes, W. (2009). Global distribution of whistler-mode chorus waves observed on the THEMIS spacecraft. *Geophys. Res. Lett.*, *36*(9), L09104. https://doi.org/10.1029/2009GL037595

Liu, Z., Mao, H. Z., Wu, C. Y., Feichtenhofer, C., Darrell, T., and Xie, S. N. (2022). A convnet for the 2020s. In *Proceedings of 2022 IEEE/CVF Conference on Computer Vision and Pattern Recognition* (pp. 11966–11976). New Orleans, LA, USA: IEEE. https://doi.org/10.1109/CVPR52688.2022.01167

McKay, D., and Kvammen, A. (2020). Auroral classification ergonomics and the implications for machine learning. *Geosci. Instrum. Methods Data Syst.*, *9*(2), 267–273. https://doi.org/10.5194/gi-9-267-2020

Mendillo, M., Baumgardner, J., and Wroten, J. (2016). SAR arcs we have seen: Evidence for variability in stable auroral red arcs. *J. Geophys. Res.: Space Phys.*, *121*(1), 245–262. https://doi.org/10.1002/2015JA021722

Nanjo, S., Nozawa, S., Yamamoto, M., Kawabata, T., Johnsen, M. G., Tsuda, T. T., and Hosokawa, K. (2022). An automated auroral detection system using deep learning: real-time operation in Tromsø, Norway. *Sci. Rep.*, *12*(1), 8038. https://doi.org/10.1038/s41598-022-11686-8

Nishimura, Y., Bortnik, J., Li, W., Thorne, R. M., Lyons, L. R., Angelopoulos, V., Mende, S. B., Bonnell, J. W., Le Contel, O., … Auster, U. (2010). Identifying the driver of pulsating aurora. *Science*, *330*(6000), 81–84. https://doi.org/10.1126/science.1193186

Nishimura, Y., Lessard, M. R., Katoh, Y., Miyoshi, Y., Grono, E., Partamies, N., Sivadas, N., Hosokawa, K., Fukizawa, M., … Kurita, S. (2020). Diffuse and pulsating aurora. *Space Sci. Rev.*, *216*(1), 4. https://doi.org/10.1007/s11214-019-0629-3

Partamies, N., Whiter, D., Kadokura, A., Kauristie, K., Nesse Tyssøy, H., Massetti, S., Stauning, P., and Raita, T. (2017). Occurrence and average behavior of pulsating aurora. *J. Geophys. Res.: Space Phys.*, *122*(5), 5606–5618. https://doi.org/10.1002/2017JA024039

Rao, J., Partamies, N., Amariutei, O., Syrjäsuo, M., and van de Sande, K. E. A. (2014). Automatic auroral detection in color all-sky camera images. *IEEE J. Sel. Top. Appl. Earth Obs. Remote Sens.*, *7*(12), 4717–4725. https://doi.org/10.1109/JSTARS.2014.2321433

Rees, M. H., and Roble, R. G. (1975). Observations and theory of the formation of stable auroral red arcs. *Rev. Geophys.*, *13*(1), 201–242. https://doi.org/10.1029/RG013i001p00201

Shang, Z. Y., Yao, Z. H., Liu, J., Xu, L. L., Xu, Y., Zhang, B. Z., Guo, R. L., and Wei, Y. (2023). Automated classification of auroral images with deep neural networks. *Universe*, *9*(2), 96. https://doi.org/10.3390/universe9020096

Shiokawa, K., Otsuka, Y., and Connors, M. (2019). Statistical study of auroral/resonant-scattering 427.8-nm emission observed at subauroral latitudes over 14 years. *J. Geophys. Res.: Space Phys.*, *124*(11), 9293–9301. https://doi.org/10.1029/2019JA026704

Størmer, C. (1929). The distribution in space of the sunlit aurora rays. *Nature*, *123*(3090), 82–83. https://doi.org/10.1038/123082b0

Syrjäsuo, M. T., and Donovan, E. F. (2002). Analysis of auroral images: Detection and tracking. *Geophysica*, *38*(1-2), 3–14.

Syrjäsuo, M. T., and Donovan, E. F. (2004). Diurnal auroral occurrence statistics obtained via machine vision. *Ann. Geophys.*, *22*(4), 1103–1113. https://doi.org/10.5194/angeo-22-1103-2004

van der Maaten, L., and Hinton, G. E. (2008). Visualizing data using t-SNE. *J. Mach. Learn. Res.*, *9*(86), 2579–2605.

Wang, Q., Liang, J. M., Hu, Z. J., Hu, H. H., Zhao, H., Hu, H. Q., Gao, X. B., and Yang, H. G. (2010). Spatial texture based automatic classification of dayside aurora in all-sky images. *J. Atmos. Sol. Terr. Phys.*, *72*(5-6), 498–508. https://doi.org/10.1016/j.jastp.2010.01.011

Yang, Q. J., Liang, J. M., Hu, Z. J., and Zhao, H. (2012). Auroral sequence representation and classification using hidden Markov models. *IEEE Trans. Geosci. Remote Sens.*, *50*(12), 5049–5060. https://doi.org/10.1109/TGRS.2012.2195667

Zhong, Y. F., Huang, R., Zhao, J., Zhao, B., and Liu, T. T. (2018). Aurora image classification based on multi-feature latent dirichlet allocation. *Remote Sens.*, *10*(2), 233. https://doi.org/10.3390/rs10020233